

RESEARCH ARTICLE | JANUARY 04 2024

Exciton and biexciton transient absorption spectra of CdSe quantum dots with varying diameters






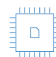
Special Collection: [Festschrift in honor of Louis E. Brus](#)

Katherine E. Shulenberger ; Skylar J. Sherman ; Madison R. Jilek ; Helena R. Keller ;
Lauren M. Pellows ; Gordana Dukovic  




J. Chem. Phys. 160, 014708 (2024)
<https://doi.org/10.1063/5.0179129>



 Nanotechnology & Materials Science  Optics & Photonics  Impedance Analysis  Scanning Probe Microscopy  Sensors  Failure Analysis & Semiconductors

Unlock the Full Spectrum.
From DC to 8.5 GHz.
Your Application. Measured.

[Find out more](#)



Exciton and biexciton transient absorption spectra of CdSe quantum dots with varying diameters

Cite as: J. Chem. Phys. 160, 014708 (2024); doi: 10.1063/5.0179129

Submitted: 29 September 2023 • Accepted: 4 December 2023 •

Published Online: 4 January 2024



View Online



Export Citation



CrossMark

Katherine E. Shulenberger,^{1,a)} Skylar J. Sherman,¹ Madison R. Jilek,¹ Helena R. Keller,²
Lauren M. Pellows,¹ and Gordana Dukovic^{1,2,3,b)}

AFFILIATIONS

¹ Department of Chemistry, University of Colorado Boulder, 215 UCB, Boulder, Colorado 80309, USA

² Materials Science and Engineering, University of Colorado Boulder, 613 UCB, Boulder, Colorado 80303, USA

³ Renewable and Sustainable Energy Institute (RASEI), University of Colorado Boulder, 027 UCB, Boulder, Colorado 80309, USA

Note: This paper is part of the JCP Festschrift in honor of Louis E. Brus.

a) Present address: Department of Chemistry, Brandeis University, 415 South Street, Waltham, Massachusetts, 02453, USA.

b) Author to whom correspondence should be addressed: gordana.dukovic@colorado.edu

ABSTRACT

Transient absorption (TA) spectroscopy of semiconductor nanocrystals (NCs) is often used for excited state population analysis, but recent results suggest that TA bleach signals associated with multiexcitons in NCs do not scale linearly with exciton multiplicity. In this manuscript, we probe the factors that determine the intensities and spectral positions of exciton and biexciton components in the TA spectra of CdSe quantum dots (QDs) of five diameters. We find that, in all cases, the peak intensity of the biexciton TA spectrum is less than 1.5 times that of the single exciton TA spectrum, in stark contrast to a commonly made assumption that this ratio is 2. The relative intensities of the biexciton and exciton TA signals at each wavelength are determined by at least two factors: the TA spectral intensity and the spectral offset between the two signals. We do not observe correlations between either of these factors and the particle diameter, but we find that both are strongly impacted by replacing the native organic surface-capping ligands with a hole-trapping ligand. These results suggest that surface trapping plays an important role in determining the absolute intensities of TA features for CdSe QDs and not just their decay kinetics. Our work highlights the role of spectral offsets and the importance of surface trapping in governing absolute TA intensities. It also conclusively demonstrates that the biexciton TA spectra of CdSe QDs at the band gap energy are less than twice as intense as those of the exciton.

Published under an exclusive license by AIP Publishing. <https://doi.org/10.1063/5.0179129>

I. INTRODUCTION

Quantifying the numbers of excitons in semiconductor nanocrystals (NCs) is critical for characterizing a variety of excited state processes, including multiexciton relaxation,^{1–5} the efficiency of carrier multiplication (multiexciton generation),^{1,6–8} the efficiencies of charge-transfer reactions,^{9–13} establishing a gain threshold for optical gain or lasing,^{14–20} and so on. Hence, considerable research efforts have been made to quantify the distribution of excited states in each NC and identify reliable spectroscopic markers for these excited state distributions.^{21–24} In transient absorption (TA) spectroscopy, multiexciton kinetics are often characterized at one

wavelength in the TA spectrum, usually the maximum of the bleach feature corresponding to the lowest-energy exciton. It is commonly assumed that the intensity of this signal is proportional to the average number of thermalized excitons, with a maximum value based on the degeneracy of the state.^{9,13,25–29} For Cd-chalcogenide NCs, the bandgap exciton degeneracy is limited by the conduction band, which has a degeneracy of 2.³⁰ Consequently, multiexciton decay is characterized under the assumption that the strength of this bleach signal scales linearly with the exciton multiplicity (i.e., a biexciton signal is twice the strength of a single exciton signal).

Recently, experimental and theoretical evidence has emerged that contradicts these assumptions.^{31,32} A single-wavelength TA study on CdSe and CdSe/ZnS quantum dots (QDs) extracted absorption cross-section ratios between the exciton to biexciton and the ground to exciton transition of between 57% and 99%, depending on the sample morphology.³³ Our group has quantitatively extracted the exciton and biexciton components in the TA spectra of CdSe QDs with a diameter of 3.0 nm and found the ratio of the biexciton and single-exciton signals at the bleach peak wavelength to be 1.6.³¹ These observations are not limited to CdSe-based QDs. The fitting of TA spectra in CsPbBr₃ NCs showed a significant size dependence on the intensity ratio of biexciton and exciton components. While the authors did not quantify this ratio, for weakly confined large NCs, the ratio appears to approach 2, and for small, confined particles, it appears to be much less than 2.³⁴ Furthermore, a recent investigation of lead-iodide perovskite NCs showed explicitly that the ground-to-exciton transition dipole moment is ~ 1.2 – $1.4\times$ larger than that of the exciton-to-biexciton transition.³⁵ While lead chalcogenide QDs have different band-edge degeneracies than the other systems discussed here (eight rather than two), the assumption that each exciton contributes equally in signal to TA bleach intensities has similarly been challenged.^{36–38} Furthermore, it has been theoretically predicted that for CdSe QDs the TA bleach peak intensity ratio for biexcitons and excitons depends weakly on size and increases with increasing QD diameter, from 1.49 for 3.0 nm QDs to 1.55 for 4.6 nm QDs.³² Additionally, the determinations of the biexciton and exciton TA component spectra for both CdSe QDs and CsPbBr₃ NCs have revealed that the widths, shapes, and peak positions can differ considerably between the two states.^{31,34} Considered together, the results reviewed in this paragraph suggest that our understanding of what determines the relative intensities of the biexciton and exciton TA signals of NCs is far from complete. For example, it is not clear: (i) What determines the peak positions and intensities of the biexciton and exciton TA component spectra? (ii) How much of the biexciton-to-exciton signal intensity ratio at a single wavelength can be attributed to the oscillator strength differences and how much to the energetic shifts between the component spectra? (iii) How do these effects depend on the particle dimensions, surface chemistry, shape, and composition?

In this manuscript, we address these questions by conducting and analyzing ultrafast TA experiments on CdSe QD samples with diameters ranging from 2.6 to 4.8 nm over a range of pump-pulse powers and timescales from 500 ps to 3 ns. Five CdSe QDs were studied with their native organic surface-capping ligands, and the 4.8 nm sample was also studied after a ligand exchange to 3-mercaptopropionic acid (3-MPA). We fit the power-dependent TA data for each sample globally to extract the biexciton lifetimes as well as the exciton and biexciton TA component spectra. The component spectra we extract represent the TA intensity if the entire ensemble could be prepared in a specific state (e.g., exciton or biexciton). We quantitatively compare the shapes and intensities of these component spectra for the different samples to understand how the exciton and biexciton TA spectral intensities vary with respect to each other and between samples. We show that the biexciton to exciton TA intensity ratio at the exciton bleach maximum, which we abbreviate as the BX:X ΔA ratio, is lower than 1.6 in all samples and does not correlate with the particle diameter. This is notable

because this ratio is usually assumed to be equal to 2.^{9,13,25–27,29} The BX:X ΔA ratio does, however, correlate with the energy difference between the bleach maxima of the exciton and biexciton component spectra, which we call the biexciton shift and abbreviate as BX shift. We also find that the BX shift, which is a measure of the biexciton interaction energy, correlates to the relative photoluminescence (PL) quantum yield (QY) of each sample, which in turn is known to be correlated with surface chemistry and, specifically, reduced by the presence of surface traps.^{39–42} This observation suggests that carrier trapping plays an important role in determining the TA spectral shapes and intensities. We test this hypothesis with the 4.8 nm QD sample that has been exchanged with 3-MPA ligands, which are known to increase trapping and quench band-gap PL.⁴³ The ligand exchange decreases the absolute intensities of the biexciton and exciton TA component spectra, increases the BX:X ΔA ratio, and decreases the BX shift, illustrating the critical role of surface chemistry in determining TA spectral shapes and absolute intensities in addition to the well-established changes in the excited state decay.^{42,44,45} We simulate predicted TA spectra from steady-state absorption spectra and conclude that while the BX shift explains the trend in our measured BX:X ΔA ratios, it cannot account for the magnitude of the values being so much lower than 2 and, therefore, the intrinsic oscillator strengths for the exciton and biexciton transitions are not determined solely by statistical factors. Our results are in overall agreement with a theoretical prediction of BX:X ΔA ratios for CdSe QDs over a similar diameter range,³² although we find that the variations due to surface chemistry effects in our experiments are wider than the predicted diameter-dependent range of BX:X ΔA ratios.

II. METHODS

A. Materials

Selenium (Se, 99.99%), trioctylphosphine oxide (TOPO, 99%), hexadecylamine (HDA, 98%), toluene (anhydrous, 99.8%), ethanol (200 proof anhydrous >99.5%), isopropanol (anhydrous, 99.5%), methanol (anhydrous, 99.8%), and chloroform (anhydrous, >99%, containing 0.5%–1% ethanol as stabilizer) were acquired from Sigma-Aldrich. Tetradecylphosphonic acid (TDPA) was acquired from PCI Synthesis. Tri-*n*-octylphosphine (TOP, 97%) and cadmium acetate (Cd acetate, 99.999%) were acquired from Strem. 3-mercaptopropionic acid (3-MPA, 99%) was acquired from Alfa Aesar. Tetramethylammonium hydroxide (TMAH, >97%) was acquired from Sigma Life Sciences.

B. CdSe QD synthesis

CdSe QDs were synthesized using a previously described procedure.⁴⁶ The synthesis and purification steps were performed under inert argon atmosphere conditions on a Schlenk line and in a glove-box, respectively. The 1.0M Se (0.79 g Se and 8.30 g TOP) and 0.17M Cd (0.12 g Cd acetate and 2.5 g TOP) precursors were prepared two days prior to the synthesis to ensure that solids were fully dissolved. The reaction solution (4.00 g TOPO, 2.50 g HDA, and 0.075 g TDPA) was placed in a three-necked round-bottom flask connected to a reflux condenser. The reaction solution was evacuated at 120 °C for 45 min. Under argon, 1 ml of the Se precursor was injected, and the solution was evacuated for a further 20 minutes. Under argon,

TABLE I. CdSe QD samples, synthesis growth times, lowest-energy exciton peak positions, and corresponding diameters.

Synthesis	Growth time	Lowest-energy exciton peak (nm)	QD diameter (nm)
S1	1 min 27 s	524	2.6
S2	37 min 0 s	566	3.4
S3	46 min 10 s	576	3.7
S4	1 h 20 min	586	4.0
S5	1 h 45 min	604	4.8

the solution temperature was then raised to 290 °C (for S1) or 300 °C (for S2–S5), and 1.5 ml of the Cd precursor was quickly injected. The growth times for each QD size can be seen in Table I above.

After growth, the reaction solution flask was cooled in a mineral oil bath. At 80 °C, the crude QD solution was placed in an argon-filled scintillation vial containing 2 ml ethanol and 8 ml chloroform and brought into the glovebox for purification. An additional 25 ml of ethanol was added, and the solution was centrifuged. The colorless supernatant was discarded, while the QD pellet was redispersed in 5 ml of toluene and centrifuged to precipitate HDA. The QD supernatant was collected in a separate vial, and these steps (redispersal of the pellet in toluene, followed by centrifugation and collection of the QD supernatant) were repeated four times; 20 ml of QD in toluene were collected in total. The QDs were precipitated with a 1:2 v/v isopropanol:ethanol mixture and centrifuged. The colorless supernatant was discarded, and the final QD pellet was dried under vacuum and redispersed in <3 ml of anhydrous toluene. CdSe QD diameter and absorption coefficients were determined from the lowest energy exciton peak using published calibration curves.⁴⁷

C. Size selection of CdSe QD S2 batch

Following the purification steps described earlier, the CdSe QD synthesis S2 resulted in relatively broad peaks in the UV–Vis absorption spectrum (supplementary material, Fig. S1) and was further purified to narrow the QD diameter distribution in the sample. Isopropanol was added dropwise to the QD stock until the solution appeared opaque, and the sample was then centrifuged. The supernatant was removed, and the pellet was dried under vacuum prior to redispersal in 1.5 ml of toluene. This fraction was then further size-selected by the same process of partial precipitation with isopropanol. The first two successive precipitations, which had overlapping absorption spectra, were dried under vacuum and combined in a total stock solution of 0.5 ml toluene to create the final S2 CdSe QDs used in the experiments described in this manuscript.

D. Ligand exchange of CdSe QD S5

A designated aliquot of CdSe QD synthesis S5 was exchanged from its native surface-capping ligands to 3-MPA ligands based on a previously reported method.^{45,48} A stock solution of 70 mM 3-MPA was prepared using 0.141 g 3-MPA, 0.456 g TMAH, and 15.0 g methanol. Roughly 30 nmol of the as-synthesized S5 QDs were suspended in <0.5 ml of toluene, precipitated with methanol, and then mixed with 1 ml of the 3-MPA stock solution. The now-exchanged QDs were precipitated using toluene and centrifuged.

The colorless supernatant was discarded, and the QD pellet was dried under vacuum and redispersed in <0.5 ml of formamide.

E. Transmission electron microscopy (TEM)

CdSe QDs TEM images were acquired using a FEI Tecnai ST20 with a LaB6 electron gun equipped with a 2k × 2k CCD and operating at 200 kV. Samples were drop-cast onto carbon-coated copper grids, 300 mesh, from Electron Microscopy Sciences. Representative images for CdSe QDs are shown in the supplementary material in Fig. S2.

F. TA spectroscopy

TA data on the five QD samples with native organic ligands were collected on a TA setup that has been described previously.⁴⁹ In summary, both the pump and probe beams were derived from a regeneratively amplified Ti:sapphire laser (Spectra-Physics, Solstice, 800 nm, ~100 fs, 1 kHz, 3.5 mJ/pulse). A fraction of the 800 nm Solstice output was tuned by an optical parametric amplifier (TOPAS-C, Light Conversion) to produce the pump beam. The white-light continuum probe beam was generated from another fraction of the 800 nm Solstice output using a sapphire plate. The TA data were collected with a HELIOS spectrometer (Ultrafast Systems). The delay time between the pump and probe pulses was controlled by a motorized delay stage, and delay times (200 fs–3 ns) were sampled with exponentially increasing step sizes, starting with an initial step size of 0.02 ps. Each time step was integrated for 0.1–1 s, depending on the signal strength at that particular excitation power. In order to extract robust error parameters at each spectral and time position, six averaged spectra were collected at each time point for each sample. TA data on the QD sample with 3-MPA ligands were collected on a similar TA system. Pump and probe beams were derived from an amplified 6 W Yb:KGW laser (Pharos PH1, Light Conversion, 1030 nm, 180 fs, 1 kHz, 1 mJ/pulse). The pump beam was generated by splitting the Pharos 1030 nm output and directing it into an optical parametric amplifier (Orpheus, Light Conversion). The probe beam was generated by directing the remainder of the Pharos 1030 nm output into a sapphire plate. TA data were collected utilizing a HELIOS Fire spectrometer (Ultrafast Systems), and all experimental parameters were held as similar as possible to the previously described system with the exception of the excitation power, which was adjusted based on the approximate pump beam spot size at the sample to generate equivalent excitation densities. Data on native-capped 4.0 nm QDs were replicated on this instrument as well to ensure that this system generated the same results as the system described above.

The QD samples were prepared with optical densities of ~0.3 at the lowest-energy exciton peak. All samples were sealed under an argon atmosphere in airtight 2 mm quartz cuvettes retrofitted with Kontes valves, and TA data were taken at room temperature. Samples were stirred continuously by a magnetic stir bar during data collection. Each sample was excited with a pump pulse at an energy of 980 meV above the band-edge absorption: 371, 391, 396, 401, and 409 nm for 2.6, 3.4, 3.7, 4.0, and 4.8 nm QDs, respectively (supplementary material, Fig. S3). These pump pulses had enough excess energy to excite above the $1P_e1P_{3/2}$ transition in each QD sample. The pump pulses were depolarized. The pump fluence

was modulated between ~ 5 and $\sim 1500 \mu\text{W}$ with continuous neutral density filters.

Before analysis, the data were corrected for scattered light and PL from the QDs as well as deviations in time zero (t_0). Scattered light and QD PL collected by the detectors were removed by averaging the pre-pump ($t < 0$) ΔA spectra and subtracting this signal from the ΔA spectra at every time point. The t_0 for an experiment is defined as the pump-probe delay time at the temporal center of the pump pulse. This value depends on the wavelength due to the chirp in the white light probe. To correct the data so that t_0 occurs at the same time point across the ΔA spectrum, TA data on a neat sample of hexanes (or formamide for the MPA-capped sample) were collected in the same TA setup with high pump fluence. The coherent response of the solvent was fit to the sum of a Gaussian, centered at t_0 , and its first and second derivatives.^{50–52} This fit was performed at several wavelengths across the probe spectrum to build a relationship between t_0 and wavelength, which was used to correct for chirp in the white light probe and, therefore, the QD TA data, by appropriately shifting the time vector.

G. PL spectroscopy

PL spectra were collected using a Fluorolog-3 spectrofluorometer (Horiba Jobin Yvon). Sample concentrations were adjusted to have an OD of 0.1 at the band edge in a $1 \times 1 \text{ cm}^2$ quartz cuvette, and the sample was kept in an air-free argon atmosphere using a custom cuvette retrofitted with a Kontes valve. Samples were excited at 450 nm with a 3 nm slit width, and PL was collected from 475 to 850 nm at a perpendicular angle from excitation with a 1 nm increment and a 3 nm slit width. The PL signal was divided by the reference intensity of the excitation beam before the sample to account for variations in source intensity and was corrected to remove the spectral dependence of detector efficiency. Relative QYs were calculated by dividing the PL intensity (determined by fitting the band-gap emission to a Gaussian and integrating) by the absorbance of each sample at 450 nm.

H. TA data analysis and fitting

1. Determination of excitation density

To control the distribution of excitons generated upon photoexcitation, we perform TA measurements over a range of pump powers. We excite each QD sample at 980 meV above the lowest-energy exciton energy, where absorption is bulk-like and therefore follows Poisson statistics.³ To extract the average number of excitons generated per QD ($\langle N \rangle$) at each power, we follow previously established procedures.^{33,37} Assuming that (1) each multiexciton state has decayed to a single exciton by 3 ns, (2) each single exciton has the same spectral intensity regardless of the initial state, and (3) exciton relaxation kinetics are independent of whether it was generated directly or via Auger recombination, we can extract the value of $\langle N \rangle$ from the TA signal at 3 ns by using the following relationship:

$$\Delta A(\lambda, 3 \text{ ns}) \propto 1 - e^{-CP}, \quad (1)$$

where $\Delta A(\lambda, 3 \text{ ns})$ is the intensity of the TA spectrum at a given wavelength at 3 ns after excitation, e^{-CP} is the fraction of QDs with zero excitations in a Poisson distribution, C is a fitting constant

that incorporates the intrinsic absorption coefficients at the excitation wavelength and the excitation spot size, and P is the excitation power. The product of C and P gives the $\langle N \rangle$ generated at each power. We fit the power dependence at the band gap bleach maximum for each QD size (supplementary material, Fig. S4). For each of the six samples studied in this work, we have plotted the initial Poisson exciton distribution for each excitation power in the supplementary material in Figs. S5–S10.

2. Extraction of exciton and biexciton TA spectra

To extract both the time constants of relaxation and component spectra for each multiexciton state, we globally fit the power-dependent TA spectra and kinetics using established Markov chain Monte Carlo (MCMC) methods.^{34,53} We adapt the software published by Ashner *et al.* (available as open source software)⁵³ to include higher order multiexcitons as introduced by Labrador and Dukovic.³¹ We choose a time window between 3 and 500 ps to eliminate contributions from hot carrier cooling at early times and non-exponential excitonic processes at late times. We chose the spectral range from 410 to 700 nm for data in Figs. 2 and 3 and 525–700 nm for data in Fig. 6 in order to incorporate spectral ranges with high signal-to-noise ratios of the white light spectrum generated by the sapphire plate and to limit the number of total data points to reduce the running time of the MCMC optimization.

The motivation and assumptions of the methods developed by Ashner *et al.* and Labrador and Dukovic are fundamentally similar. We describe these assumptions and discuss their accuracy in the CdSe QD system investigated here. First, multiexcitons recombine in a ladder-like cascade where triexcitons recombine to biexcitons, biexcitons recombine to single excitons, and single excitons recombine to the ground state. This ladder-like recombination of multiexcitons has been established previously.^{21,22,54} Second, each of these processes is a first-order kinetic process with a unique rate constant. While this assumption is not entirely valid for the single exciton due to the presence of electron and hole traps, throughout the time range being fit (3–500 ps), the single exciton decay can be well approximated as a single exponential. Labrador and Dukovic illustrated that a wider time range can be fit by accounting for the exciton lifetime with a biexponential process, but the inclusion of this additional rate component did not alter the component spectra that were extracted.³¹ Therefore, for the sake of the efficiency of the fitting algorithm, we have excluded this complication. Third, we assume that each excitonic state has the same TA spectrum and relaxation kinetics, regardless of the initial state of the system. For CdSe QDs, the lack of memory in the system has been previously established in PL measurements.⁵⁴ Finally, we assume that at each point in time, the total TA spectrum is a linear combination of the component spectra weighted by the population of that state (exciton, biexciton, and triexciton). In our dilute solution-phase environment, it is unlikely that any interparticle interactions exist that would invalidate this assumption.

The output of the MCMC fits are four system parameters: the triexciton lifetime, biexciton lifetime, exciton lifetime, and the “ C ” parameter [Eq. (1)], which accounts for spot size and particle absorption coefficients. The error on these coefficients is reported as the standard deviation of the values output from the Markov chain. We also extract the TA component spectra for the exciton, biexciton, and triexciton. These component spectra are quantitative for

the given sample concentration. For example, the exciton component spectrum is the change in absorbance between an ensemble of QDs entirely in the ground state and entirely in the single exciton state. Due to the breadth of the Poisson distribution at high excitation densities, the triexciton spectrum contains contributions from multiple higher order multiexcitons, and thus we will not further interpret these spectra.

We illustrate the robustness of the fits by plotting the residual between the modeled spectral evolution and the raw data in Figs. S11–S16 of the supplementary material. Across all powers, the relative error in the fits is very low, demonstrating the accuracy and lack of bias in the extracted spectra. We also show the correlation plots between the kinetic and Poisson parameters as performed by Ashner *et al.* in the supplementary material in Figs. S17–S22.^{34,53} The lack of a strong correlation between the extracted parameters suggests that the kinetic model is appropriate and not overly parameterized.

III. RESULTS AND DISCUSSION

A. Relevant excitonic transitions in the five CdSe QD samples

In this study, we use CdSe QDs synthesized with native long-chain organic surface-capping ligands according to previously reported methods as described in Sec. II B. By varying the particle growth time, we obtained five QD batches with diameters of 2.6, 3.4, 3.7, 4.0, and 4.8 nm, whose steady-state absorption spectra are shown in Fig. 1(a). The resulting CdSe QD diameters were 2.6, 3.4, 3.7, 4.0, and 4.8 nm.

The three lowest-energy excitonic absorbing states in CdSe QDs are $1S_e1S_{3/2}$, $1S_e2S_{3/2}$, and $1P_e1P_{3/2}$, which we abbreviate as the 1S, 2S, and 1P transitions.^{55–57} The relative energy levels of these

transitions are represented schematically in Fig. 1(b). These transitions are shown for the steady-state absorption and TA spectra of the 3.7 nm QDs in Fig. 1(c) and the other four QD samples in the supplementary material in Fig. S23. Of particular interest to this work are the two lowest energy transitions (1S and 2S), since both states will be at least partially occupied by the presence of a band-edge photoexcited electron ($1S_e$ state).

We quantify the intensities, spectral positions, and peak widths of the 1S, 2S, and 1P absorption transitions in each CdSe QD sample by fitting the steady-state absorption spectra to three Gaussians (supplementary material, Fig. S24). These fits are particularly important for understanding how absorption changes with the presence of excitons, and detailed comparisons with these steady-state optical properties will be made in Secs. III B, III D, and III E. All three states show the expected redshifts in energy with increasing QD diameter [Fig. 1(d) for 1S and 2S transitions, supplementary material, Fig. S25(a) for the 1P transition]. The difference between the 1S and 2S peak energies decreases linearly with increasing QD diameter from ~ 160 – 110 meV, going from 2.6 nm QDs to 4.8 nm QDs, respectively (supplementary material, Fig. S26). The samples were prepared to have an absorbance of ~ 0.3 at the band-edge 1S exciton feature. Accordingly, the peak intensity of each of these is roughly equivalent [Fig. 1(e), squares]. The relative peak intensity of the 2S transition [Fig. 1(e), circles] increases with increasing QD diameter, while the intensity of the 1P transition does not have a clear size dependence [supplementary material, Fig. S25(b)]. Additionally, the QDs have, on average, broader features for each state as QD size decreases [Fig. 1(f) and supplementary material, Fig. S25(c)]. To examine the contributions of the 2S state to the band-edge (1S) absorption, we calculate the relative intensity of the 2S curve at the 1S peak wavelength (supplementary material, Fig. S27). Regardless of particle size, the contribution of the 2S absorption to the 1S peak

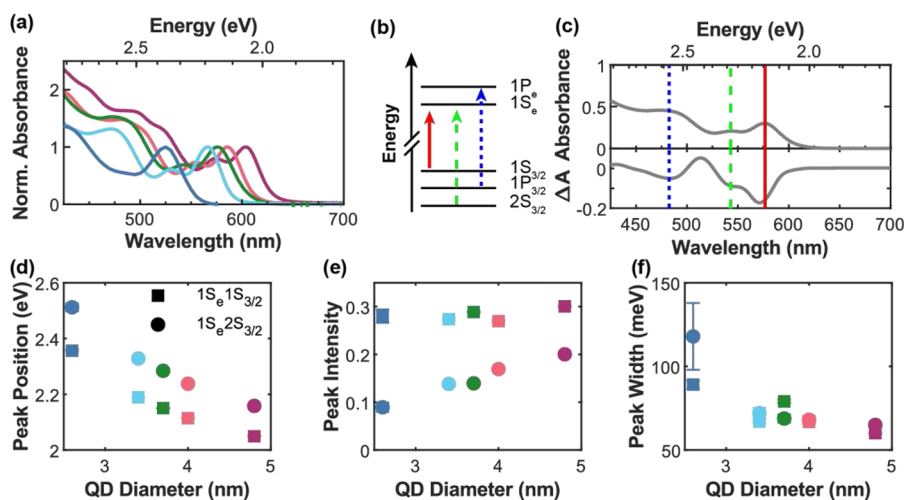


FIG. 1. (a) Steady-state absorption spectra of the five CdSe QD samples. 2.6, 3.4, 3.7, 4.0, and 4.8 nm QDs are shown in blue, cyan, green, orange, and magenta, respectively. (b) The $1S_e1S_{3/2}$ (1S), $1S_e2S_{3/2}$ (2S), and $1P_e1P_{3/2}$ (1P) QD absorbing states are marked on the spectra in (c) with the red solid, green dashed, and blue dotted lines, respectively. Relative energy levels are not shown to scale. (c) The peak positions of the $1S_e1S_{3/2}$ (1S), $1S_e2S_{3/2}$ (2S), and $1P_e1P_{3/2}$ (1P) states in the steady-state absorption and TA spectra of one of the QD sizes (3.7 nm). (d)–(f) The fitted peak position, peak intensity, and peak width for the 1S and 2S Gaussian absorption features for each of the five QD sizes.

absorption in the ground state absorption spectrum is quite small (<6%), suggesting that the difference in the bleach intensities of the 1S and 2S features should play a minimal role in determining the TA intensity at the band edge.

B. Exciton and biexciton spectra component spectra from TA data with varying pump power

To extract the TA component spectra that correspond to excitons and biexcitons in the five CdSe QD samples, we performed TA measurements with 8–12 pump powers, ranging from the mostly single exciton regime ($\langle N \rangle \sim 0.03$) to an $\langle N \rangle$ of ~ 2 (Fig. 2). The determination of $\langle N \rangle$ is described in Sec. II H 1. A large excess photon energy (980 meV above the 1S peak) was selected to ensure that absorption is through predominantly bulk states that obey Poisson statistics in exciton distribution,³ that the 1P exciton transition is to the red of the pump photon energy, and that hot carrier effects are similar for all of the QD sizes studied here. The pump pulse spectra are shown overlaid with the steady-state absorption spectra of the five QD samples in the supplementary material in Fig. S3.

First, we examine the results of these experiments qualitatively. In Figs. 2(a)–2(e), we show the TA spectra measured at the pump-probe delay of 3 ps for the five CdSe QD samples at varying pump powers with the intensity of the bleach signal normalized at the 1S peak. In the low photon flux regime ($\langle N \rangle < 0.1$), spectral shapes are the same, consistent with increasing numbers of QDs in the ensemble with single excitons but no appreciable population of multiexcitons. Moving above $\langle N \rangle \sim 0.1$, the spectral signatures of multiexcitons begin to emerge. For each sample, with increasing $\langle N \rangle$, we observe a slight redshift in the bandgap bleach, a loss of the induced absorption on the red edge of the bandgap bleach, and a redshift and some bleaching of the 1P energy level. At the highest excitation powers ($\langle N \rangle > 1$), we also observe an increasing bleach of the 1P level, corresponding to the presence of higher order multiexcitons. These spectral changes were previously described for CdSe QDs with a 3.0 nm diameter and were attributed to increasing spectral contributions of the biexciton and triexciton species to the TA spectrum with increasing $\langle N \rangle$.³¹

In Figs. 2(f)–2(j), we show the kinetics of the 1S bleach peak for all the samples and powers, normalized at 3 ns. For all QD sizes, as the excitation power increases, we observe additional fast components in the bleach decay. The presence of multiexcitons at early times does not change the late time (exciton) kinetics, which all collapse to the same functional form by ~ 300 ps. The enhancement of the relative intensity of these fast lifetime components with increasing excitation power is a well-established phenomenon assigned to nonradiative Auger recombination of multiexciton states.^{21,22} After the Auger recombination is complete, the remaining single excitons have overlapping associated decay kinetics.

To extract the exciton and biexciton TA component spectra from the data in Fig. 2, we use global fitting procedures that extract the multiexciton lifetimes and component spectra, as detailed in Sec. II H 2. In summary, we assume that the initial populations at each excitation power are related by the spot size and QD absorption coefficient, that the average number of excitons generated is linear with the excitation power, and that the excitations follow a Poisson distribution of multiexciton states. The complete power-dependent TA dataset for each sample is input into an optimization algorithm

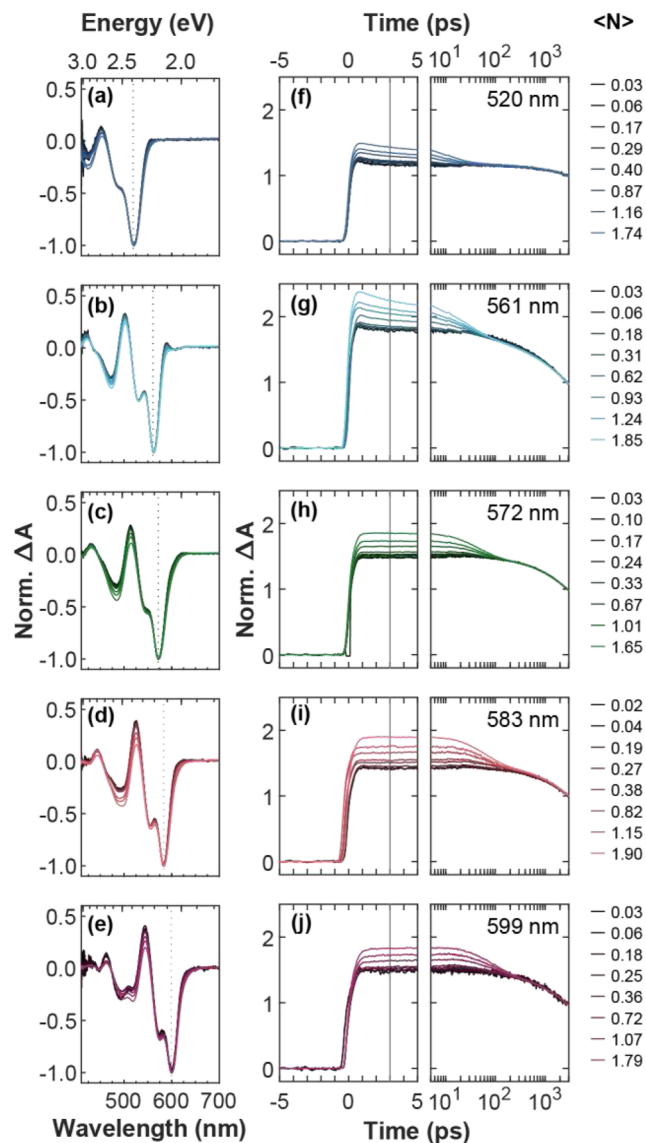


FIG. 2. (a)–(e) For each of the five QD sizes, we extract the normalized TA spectrum at 3 ps after photoexcitation at several excitation powers. The bleach maximum is at 520, 561, 572, 583, and 599 nm for the 2.6, 3.4, 3.7, 4.0, and 4.8 nm QDs, respectively. (f)–(j) We show the corresponding recombination kinetics at the exciton bleach maximum at several excitation powers, ranging from an average excitation rate of <0.05 per QD to >1.5 per QD. The first 5 ps are shown on a linear-time axis, and the subsequent 3 ns are shown on a log-time axis. Traces are normalized at 3 ns to compare the differences in kinetics during multiexciton recombination.

that assumes that each TA spectrum at every time and excitation power is a linear combination of intrinsic component spectra for each excitonic state and that these states each have exponential decays. The global parameters, which are extracted using an MCMC algorithm, are the lifetimes for each state (i.e., exciton, biexciton, and triexciton) and the C parameter, which contains the spot size and absorption coefficient. The component spectra are determined

using a linear least squares optimization given the four global parameters during each iteration. For the smallest QD size (2.6 nm), the triexciton lifetime is sufficiently short that the sample has decayed to biexcitons and excitons exclusively by 3 ps, and therefore, only the biexciton fitting algorithm was used for this sample.

The extracted biexciton lifetimes for the five CdSe QD samples are plotted as a function of QD volume in Fig. S28 of the supplementary material. These lifetimes range from 11.800 ± 0.005 ps for the smallest QDs to 57.38 ± 0.03 ps for the largest and show linear scaling with volume, consistent with the established understanding of Auger recombination in QDs.^{3,58} We also extract triexciton lifetimes for the larger QD samples. These triexciton lifetimes range from 2 to 7 ps. However, due to the increasing breadth of the Poisson distribution at higher excitation densities (supplementary material, Figs. S5–S10), the triexciton lifetime likely convolves multiple higher order multiexciton states and, therefore, we will not further analyze these lifetimes.

The exciton and biexciton TA component spectra for each of the five QD sizes are shown in Figs. 3(a)–3(e). These spectra are absolute in intensity, meaning that they represent the TA spectra that would be measured if a sample consisted of QDs that all had exactly an exciton or biexciton, respectively. In the exciton TA spectra, we note a weak induced absorption on the red-edge of the bandgap bleach maximum. This is because the exciton TA spectrum contains a bleach of the ground-to-exciton transition and an

induced absorption, which corresponds to the exciton-to-biexciton transition.^{23,59–64} The redshift of the exciton-to-biexciton absorption relative to the ground-to-exciton absorption transition results in a small induced absorption. For the biexciton component spectrum, we observe no such induced absorption. This is because the conduction band edge is saturated with electrons and, therefore, there is no further absorption of the bandgap energy. This is consistent with the qualitative observations made in Figs. 2(a)–2(e), where low power spectra at 3 ps show an induced absorption at the red edge of the bleach, but at higher excitation powers, where an appreciable fraction of excited states are multiexcitons, we observe no such induced absorption.

We also observe a redshift of the bleach maximum for the biexciton spectrum as compared to the exciton spectrum in all QD sizes, consistent with the qualitative observation that the bandgap bleach redshifts with increasing excitation power. We define the energy difference between the positions of the two bleach maxima as the BX shift (not to be confused with the biexciton binding energy).⁶⁵ The BX shift will increase with increasing biexciton interaction energy because the biexciton interaction shifts exciton absorption energies, therefore shifting the bleach maxima of the ΔA spectra.²¹ Interestingly, the BX shift does not correlate with the particle diameter (supplementary material, Fig. S29), suggesting that the particle dimension is not the dominant determinant of the biexciton interaction energy and that other properties play an important role, as we address later in the text (Sec. III C).

Figure 3 makes it immediately obvious that the intensity ratio between the biexciton and exciton TA component spectra at the bleach maximum of the ensemble TA spectrum (which we abbreviate as “BX:X ΔA ratio”) is not 2, as is commonly assumed,^{9,13,25–27,29} but a number lower than that. The wavelength at which we extracted the BX:X ΔA ratio is marked by the gray dashed line in Figs. 3(a)–3(e) for each QD size. (The biexciton-to-exciton TA intensity ratio as a function of wavelength is shown in Fig. S30 in the supplementary material.) The extracted values of the BX:X ΔA ratio at the bleach maximum range from 1.37 to 1.48. We do not observe a correlation between this value and the QD diameter [Fig. 4(a)]. We do observe an inverse correlation between the BX:X ΔA ratio and the magnitude of the BX shift [Fig. 4(b)]. This correlation is not surprising because the separation between the biexciton and exciton bleach peaks leads to the biexciton bleach signal being farther away from its maximum at the ensemble bleach maximum, reducing the BX:X ΔA ratio. In other words, the value of the BX:X ΔA ratio is determined by both the “intrinsic” intensities of the biexciton and exciton TA component spectra and the value of the BX shift. Theoretically predicted values of the BX:X ΔA ratio are also shown in Fig. 4(b) and will be discussed in Sec. III D.³²

C. Surface effects in exciton and biexciton TA component spectra

Given that neither the BX shift nor the BX:X ΔA ratios correlate with the QD diameter for our five samples [Fig. 4(a) and supplementary material, Fig. S29], we hypothesize that the QD surface chemistry, and in particular fast (compared to the Auger recombination timescale) surface carrier trapping, may play an important role in determining the values of both parameters. PL QY has been shown to report on the degree of trapping in QDs.⁶⁶

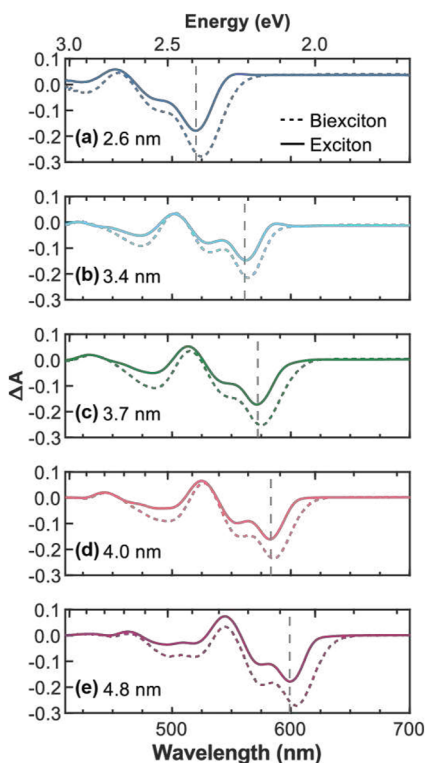


FIG. 3. (a)–(e) Exciton (solid) and biexciton (dotted) TA component spectra for 2.6, 3.4, 3.7, 4.0, and 4.8 nm CdSe QDs, respectively. The exciton bandgap bleach maximum is marked by the gray dashed line in each sample as a guide to the eye.

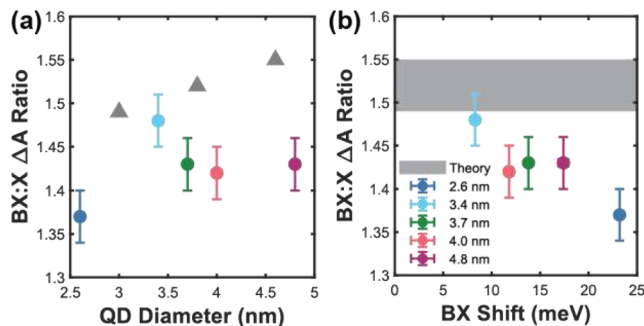


FIG. 4. Biexciton to exciton TA intensity ratio at the exciton bleach maxima for each of the five CdSe QD sizes as a function of the (a) QD diameter and (b) BX shift. The colors correspond to the particle diameter, with blue being 2.6 nm, cyan 3.4 nm, green 3.7 nm, orange 4.0 nm, and magenta 4.8 nm. The gray triangles in (a) and the gray shaded region in (b) represent the range previously reported from theoretical predictions for CdSe QDs with diameters from 3.0 to 4.6 nm and will be discussed in Sec. III D.³² The error in the BX:X ΔA ratio, which we estimate to be ± 0.03 predominantly arises from uncertainty in the laser power measurement, not uncertainty in the MCMC optimization, which we estimate to be ± 0.03 .

The dominant pathway reducing bandgap PL QY^{39–42} is the fast (ps timescale)^{67–73} trapping of valence band holes. The PL spectra of the five samples [Fig. 5(a), inset] show bandgap exciton emission peaks that are roughly Gaussian. We fit these exciton emission features and calculate relative exciton PL QY values as described in Sec. II G. The relative exciton PL QY does not correlate with the QD diameter [Fig. 5(a)]. We note that the sample with the lowest PL QY, the 3.4 nm QDs, was size-selected via additional precipitation steps with isopropanol (Sec. II C), likely introducing additional trap states to the QD surface.^{41,74} Figure 5(b) shows the relative

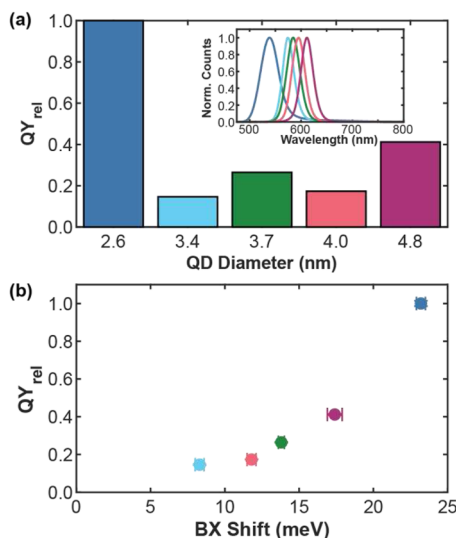


FIG. 5. (a) Relative PL QYs of the five CdSe QD samples calculated from the area under the band-edge emission feature of the unnormalized spectra. Inset: Normalized PL spectra of the five CdSe QD samples. (b) The relative PL QYs shown in panel (a) plotted against the BX shift for each QD sample.

PL QY as a function of the BX shift calculated from the TA component spectra shown in Fig. 3. The correlation between the two values suggests that surface trapping plays a role in determining the BX shift. Because higher BX shifts indicate a higher biexciton interaction energy, this correlation suggests that the biexciton interactions involving trapped carriers are weaker than those involving band-edge carriers, presumably due to reduced Coulomb interactions when a carrier is on the surface rather than delocalized in the QD.

We test the importance of surface trapping in determining the BX shift suggested by Fig. 5(b), as well as its role in TA component spectral intensities, by carrying out TA experiments on a QD sample with more efficient hole trapping. We prepared this sample by ligand exchanging the 4.8 nm QDs from the native long-chain organic ligands to 3-MPA ligands, which are known to quench the PL QY and introduce additional hole traps to the NC surface.^{43,75–77} After ligand exchange, these QDs show no detectable PL, confirming the high degree of hole trapping, which results in excitons that consist of valence band electrons and trapped holes. The fraction of these excitons is higher in the 3-MPA capped QD sample than in the sample with native ligands. The absorption spectra of the pre- and post-exchange particles in hexanes and formamide, respectively, are shown in Fig. 6(a).

We performed TA measurements on this ligand-exchanged QD sample over a range of pump powers (supplementary material, Fig. S31) to fit the biexciton lifetime and extract the TA component spectra. The biexciton lifetime of these 3-MPA-capped QDs is similar to that of the native-ligand-capped QDs (69 and 57 ps,

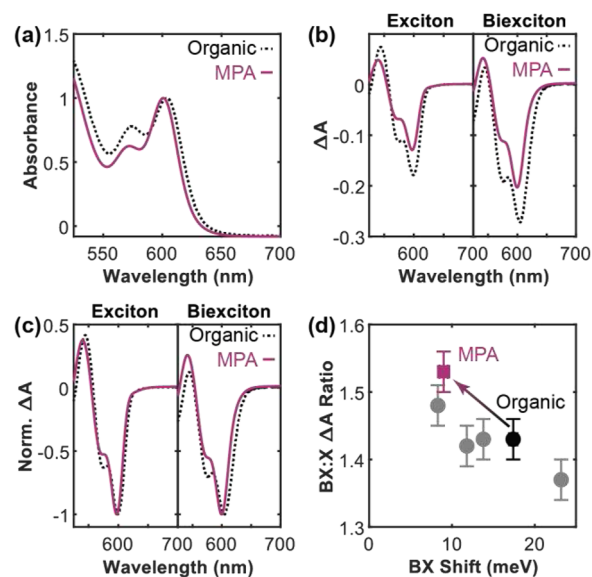


FIG. 6. (a) Normalized absorbance spectra of 4.8 nm CdSe QDs with native TDPA/HDA ligands (black) and 3-MPA ligands (magenta). (b) Exciton and biexciton component spectra for the two samples shown in (a). (c) The same component spectra shown in (b), normalized at the bleach maximum. (d) The BX:X ΔA ratio at the exciton bleach maximum for the five native ligand samples (gray), with the 4.8 nm sample highlighted in black. The ligand-exchanged 3-MPA-capped 4.8 nm QDs are shown in magenta.

respectively). In Fig. 6(b), we compare the extracted exciton and biexciton TA component spectra before and after ligand exchange. The extracted spectra for both the exciton and biexciton components are weaker in magnitude for the 3-MPA-capped particles than the native-ligand-capped particles. Recall that these component spectra are absolute in intensity, meaning that they represent the TA spectra if a sample could be prepared with every QD in the same excited state. This result is consistent with the recent literature reports that suggest that fast (~ 1 ps) hole trapping removes the valence-band hole contribution to the bandgap bleach of CdSe QDs.^{78,79} (Recall that our data analysis starts at 3 ps and would, therefore, capture the spectra of QDs with trapped holes.) The data in Fig. 6(b) illustrate the importance of fast carrier-trapping in determining the “intrinsic” intensities of the biexciton and exciton TA component spectra.

In Fig. 6(c), we compare the exciton and biexciton TA component spectra of the QDs with the native ligands and 3-MPA ligands by normalizing them at their respective bleach maxima. The exciton component spectra show similar 1S bleach peak positions in both samples. The biexciton component spectra show a larger difference in the 1S bleach maximum position between the two samples than the exciton spectra, with the 3-MPA sample being blue-shifted. In Fig. 6(d), we add the BX:X ΔA ratio for the 3-MPA-capped QDs as a function of the BX shift to the data on the five native ligand-capped QD samples. Along with the decreased BX shift for 3-MPA capped particles, we observe an increase in the BX:X ΔA ratio. As stated earlier, we suspect that the BX shift is smaller because the electron-hole interaction is weaker when the hole is trapped, resulting in a reduced BX binding energy, manifesting in a reduced shift in the TA spectra. These changes in intensities, relative intensities, peak positions, and relative peak positions of exciton and biexciton TA component spectra upon ligand exchange demonstrate the importance of fast carrier trapping in determining the absolute TA spectra of CdSe QDs. We conclude that these absolute spectra are strongly influenced by the surface chemistry rather than being intrinsic to a particular QD composition, size, and shape and are, therefore, likely to vary from sample to sample in ways that are not straightforward to predict. This strong impact of surface chemistry likely creates discrepancies in the relative exciton and biexciton TA spectral intensities between different studies, as small changes in sample synthesis and preparation may create relatively large differences in the observed spectral intensities.

We have thus far illustrated that changes in the BX shift due to surface chemistry alterations contribute to the differences in BX:X ΔA ratios measured in our TA data. However, the BX shift alone cannot account for the ratio of biexciton and exciton TA signals being less than 2. A linear extrapolation to zero BX shift across the trend in the five samples with native organic ligands, shown in Fig. S32 in the supplementary material, leads to a BX:X ΔA ratio of ~ 1.55 . We, therefore, next examine the factors that contribute to the intensities of the TA spectra.

D. Oscillator strengths of exciton and biexciton transitions

In order to model the expected exciton and biexciton components in the TA spectra, we must first understand what signals contribute to the measured TA spectral components. We illustrate the contributions to the TA component spectra in Fig. 7(a). For

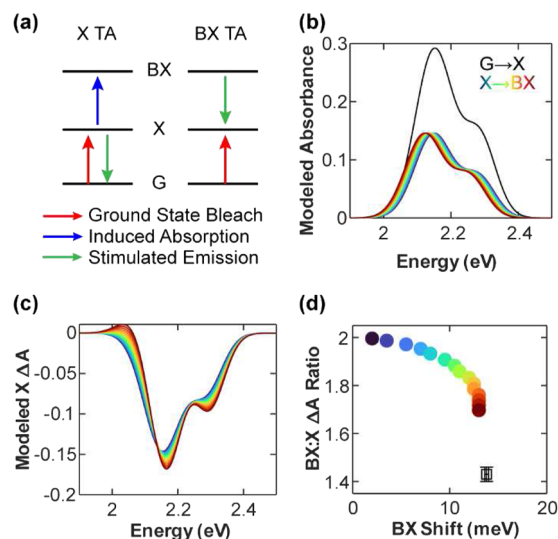


FIG. 7. (a) Schematic representation of the contributions from band-edge states to the exciton and biexciton TA component spectra. (b) Simulated ground-state absorption (black) and exciton absorption (colors) for the 3.7 nm QDs with an exciton shift relative to the ground state absorption increasing from blue to red. The range of shifts modeled is from 0 to 30 meV. (c) The resultant exciton TA spectra for each of the exciton absorption spectra shown in (b). It is assumed there are no contributions from SE. (d) The BX:X ΔA ratio at the band edge for each of the exciton TA spectra modeled in (c). The measured value is shown in black.

simplicity, we only consider the two lowest energy exciton transitions (1S, 2S) here. Recall that a TA spectrum is the change in the absorption of the sample in the presence of the pump excitation. When each particle has a single exciton, due to pump absorption or multiexciton relaxation, the probe light excites the transition from the existing exciton (X) to the biexciton (BX) state. There is also stimulated emission (SE) from the exciton (X) to the ground state (G). With the pump off, the probe excites the G → X transition exclusively. This leads to an exciton TA component spectrum with three primary contributions: (1) a bleach of the G → X for both the 1S and 2S transitions [Fig. 7(a), red], (2) an induced absorption for the X → BX transition at the 1S and 2S transition [Fig. 7(a), blue], which in our samples is redshifted from the G → X transition, and (3) SE from the cooled 1S state back to the ground state [Fig. 7(a), green]. The biexciton TA component spectrum has two possible contributions: (1) the bleach of the G → X 1S and 2S transitions, and (2) SE from the BX → X states. Since the degeneracy of the 1S_e electron level is two, there is no induced absorption corresponding to the BX → TX (triexciton) transition for either the 1S or 2S state. As a result, the biexciton TA component spectrum has a stronger bleach signal than the exciton TA component spectrum. With a doubly degenerate CB and without any other factors influencing the absorption strength, a single exciton would bleach exactly half of the available transitions from the VB to the CB, and a biexciton would fully bleach the transition. In other words, the G → X transition would be exactly twice as strong as the X → BX transition, and the biexciton TA bleach would be exactly twice as intense, resulting in the commonly assumed ratio of 2.

To simulate the TA spectra using these relationships, we first examine the expected contribution from the SE. We estimate the SE contribution by calculating the individual steady-state absorption spectra for the exciton and biexciton states and adding their respective TA component spectra to the overall steady-state absorption spectrum (Fig. S33). When a state has a net SE, it will manifest as a steady-state absorption signal that is less than zero¹⁵ because there is more light exiting the sample than was incident upon it. We only detect this SE signature in the largest QD sizes in the biexciton, but not exciton, absorption spectra (Fig. S33). Therefore, neglecting SE from the simulated exciton TA component spectra is a reasonable assumption for all the samples, and from the simulated biexciton TA component spectra for all but the 4.8 nm and possibly the 4.0 nm QD samples. The lack of SE from core-only CdSe QDs, which have significant hole trapping and relatively low PL QY, is well known in the literature.^{39,80,81} Furthermore, SE from the biexciton state in the larger diameter (4.0 and 4.8 nm) samples will increase the bleach intensity in the biexciton TA component spectrum. An increase in the magnitude of the biexciton TA component spectrum as compared to the exciton TA component spectrum results in an increase in the BX:X ΔA ratio. Therefore, the ratio we simulate is a lower bound to the ratio excluding changes in absorption strength. Since SE is included in our measured data, the difference between our simulated BX:X ΔA ratio and the measured value is the minimum contribution required from a change in absorption strength. We, therefore, proceed with our analysis by ignoring SE.

We generate the simulated TA component spectra by starting with the fitted 1S and 2S steady-state absorption transitions from main text Figs. 1(d)–1(f). These spectra [e.g., Fig. 7(b), black] correspond to the $G \rightarrow X$ absorption transition, which is fully bleached in both the exciton and biexciton TA component spectra. We next generate steady-state absorption spectra for the $X \rightarrow BX$ transition in a hypothetical sample of QDs with single excitons, with different energetic shifts between the $G \rightarrow X$ and $X \rightarrow BX$ transitions. Recall that our goal is to test whether the BX:X ΔA ratios we measure can be produced by the BX shift alone when the $G \rightarrow X$ transition is exactly twice as strong as the $X \rightarrow BX$ transition. Therefore, we assume the strength of the $X \rightarrow BX$ absorption is exactly $1/2$ that of the $G \rightarrow X$ absorption and then shift the absorption energy of both the 1S and 2S transitions linearly between 0 and 30 meV. It is useful to note that this is the shift in the steady-state absorption energies, while the BX shift is an effect observed in the difference spectra, which includes impacts from a number of factors. For simplicity, we assume 1S and 2S states shift the same amount. We selected the range of shifts between the $G \rightarrow X$ and $X \rightarrow BX$ absorption spectra [Fig. 7(b), blue to red] to be 0–30 meV, which covers the expected range of values from previous measurements of the biexciton binding energy in CdSe QDs.^{23,63,82–88} While larger shifts than those shown in Figs. 7(b) and 7(c) would continue to reduce the BX:X ΔA ratio, the spectral shape we observe would be inconsistent with anomalously large shifts since we only see a weak induced absorption to the red of the 1S exciton feature. Large BX binding energies would result in a large magnitude of induced absorption in the TA spectra, which is not seen in our data (Fig. S34). By taking the difference between the $G \rightarrow X$ absorption and the $X \rightarrow BX$ absorption shown in Fig. 7(b), we generate the simulated exciton TA component spectra [Fig. 7(c)]. The simulated biexciton TA component spectrum for band-edge transitions is simply the negative of the $G \rightarrow X$ absorption [Fig. 7(b), black].

From these simulated TA component spectra, we can extract the expected values of the BX shift and the BX:X ΔA ratio. We plot these values in Fig. 7(d) and compare them to the measured value for this sample (3.4 nm QDs). We show the same simulated ratios for the other four QD sizes in Fig. S35. Across all samples, the values of the BX:X ΔA ratio in the simulated range are considerably larger than the experimentally measured values in Fig. 4. Additionally, recall that we excluded contributions from SE when simulating our TA component spectra. Including SE would increase the simulated ratios even further away from the experimental data due to the stronger SE from the biexciton state than the exciton. The differences that we observe between the measured and simulated BX:X ΔA ratio values are the lower limit. We can, therefore, definitively conclude that the intrinsic BX:X ΔA ratio is intrinsically less than 2 in CdSe QDs and, therefore, the presence of an exciton will reduce the oscillator strength of the $X \rightarrow BX$ transition relative to the $G \rightarrow X$ transition by more than just statistical factors.

E. BX:X ΔA ratio values in the context of prior literature

Our results illustrate that discrete excitonic absorption transitions in CdSe QDs have absorption coefficients that depend upon the number of excited carriers in the QD beyond the known statistical factors. This is in contrast to assumptions often made when measuring the number of multiexciton states per NC under particular excitation conditions. For example, when quantifying the efficiency of multiexciton generation in CdSe QDs using single-wavelength TA, a fundamental assumption is that the biexciton has exactly twice the bleach signal as the exciton at the bleach maximum.^{9,25–27,29} Here, we have shown that for a set of samples that are fundamentally similar (e.g., same solvent, ligand, synthesis procedure), the BX:X ΔA ratio varies with respect to material parameters beyond just the QD diameter and is, under all conditions examined here, significantly less than 2. This suggests that previously measured multiexciton generation efficiencies underestimate the number of excitons generated. The pump-power-dependent TA measurements and global fitting described here can rigorously quantify the number of excitons or biexcitons in a QD present at different time points of the excited state decay.

Our observations are in general agreement with the theoretical prediction of Franceschetti and Zhang in CdSe QDs of 3.0–4.6 nm diameter, where the calculated BX:X ΔA ratio is 1.49–1.55 at room temperature (Fig. 4).³² These calculations took into consideration only core states and did not account for trapping or SE. Nevertheless, the resulting BX:X ΔA ratios are within the error of our measured values [Figs. 4 and 6(d)]. The authors ascribe the BX:X ΔA ratios to two root causes, similar to those we discuss in this manuscript (Sec. III D): energy shifting and changes in oscillator strength, both of which they attribute to exciton–exciton interactions.^{32,89,90}

Franceschetti and Zhang further predict that the presence of an exciton in the system will decrease not just the oscillator strength of the occupied transition (in this case 1S and 2S) but also unoccupied states (e.g., 1P).³² We observe this reduction in the absorption coefficient for higher order excitonic transitions (e.g., 1P) (see arrow in supplementary material, Fig. S35) in almost quantitative agreement with their prediction. Effective mass approximation modeling of NCs by Takagahara, which explicitly includes both quantum

confinement and dielectric confinement, suggests that the change in the NC dielectric constant in the presence of an exciton contributes strongly to the changes in the oscillator strengths of other transitions.³¹ Our observed changes in oscillator strength of not just the occupied states (Fig. S35), but all excitonic states in the QDs, are consistent with this prediction.

The largest difference between the predictions and our measured results is in the size dependence. We do not observe the weak increase of the BX:X ΔA ratio with increasing particle diameter predicted by Franceschetti and Zhang.³² The predicted size dependence is relatively small and similar in magnitude to our estimated error in the BX:X ΔA ratio, so our experiments may not be sensitive enough to observe such a size dependence. Moreover, the range of values we measure is wider, and the impact of surface traps on the BX:X ΔA ratio, described in Sec. III C, is significant. Theoretical results only considered band-edge carriers. Therefore, while there may be a weak underlying impact of the QD size on the BX:X ΔA ratio, we conclude that it is smaller in magnitude than the effects induced by differences in the BX shift from trapped carriers. We expect that for heterostructure materials with minimal surface hole-trapping, a weak size dependence of the BX:X ΔA ratio may emerge.

IV. CONCLUSIONS

In summary, we described a detailed investigation of TA spectroscopy measurements on CdSe QD samples carried out over a range of pump-pulse powers. We analyzed five CdSe QD samples, with diameters ranging between 2.6 and 4.8 nm, all capped with their native organic surface-capping ligands, as well as the 4.8 nm QD sample that was ligand exchanged to 3-MPA. By globally fitting the pump power series for each sample, we extracted biexciton lifetimes as well as exciton and biexciton TA component spectra. The isolated component spectra represent the TA intensity if all ensemble components were prepared in that particular state. We examined the spectral shapes, positions, and intensities to reveal how they vary among each other and across different samples. We found that the BX:X ΔA ratio does not correlate with particle diameter but does correlate inversely with the BX shift, which in turn correlates with relative PL QY. In other words, lower relative PL QY, which indicates a higher degree of carrier trapping, also leads to a smaller BX shift and, therefore, a reduced biexciton interaction, which contributes to a relatively higher BX:X ΔA ratio, presumably because of improved overlap of exciton and biexciton peak positions. We further examined the role of surface trapping with a 4.8 nm QD sample that underwent ligand exchange to 3-MPA ligands, which are known to increase hole trapping. The ligand exchange led to noticeable changes in the absolute intensities of the biexciton and exciton component spectra and resulted in an increased BX:X ΔA ratio and a decreased BX shift. By extrapolating the effect of the BX shift to zero, we found the BX:X ΔA ratio was well below 2 across all samples, even with the absence of spectral shifts. The magnitude of the observed BX:X ΔA ratio is similar to theoretical predictions, but the range of values is broader than the predicted range, presumably because variations due to surface trapping are larger than variations due to QD diameter. In the broader context, our work highlights how surface-related phenomena impact the intensities and shapes of TA spectra of QDs and demonstrates that the presence of an exciton in a

particular near-bandgap state reduces the intensity of the subsequent absorption transitions.

SUPPLEMENTARY MATERIAL

See the supplementary material for material characterization, TA fitting, UV-Vis fitting, TA fitting results and further analysis, and simulation of transient absorption spectra.

ACKNOWLEDGMENTS

This work was supported primarily by the Air Force Office of Scientific Research under AFOSR Award Nos. FA9550-19-1-0083 and FA9550-22-1-0347. K.E.S. also acknowledges support from the National Science Foundation Grant No. CHE-2125978 awarded to the Research Corporation for Science Advancement for the Cottrell Fellowships Award No. 27980. M.R.J. and H.R.K. acknowledge support from the National Science Foundation Graduate Research Fellowship Program under Award Nos. DGE 2040434 and DGE 1650115, respectively. TEM imaging was supported by the National Science Foundation under STROBE Grant No. DMR 1548924. The data in Figs. 6 and S32 were collected in part using the ultrafast optical biophysics facility and laboratory, located at the National Renewable Energy Laboratory, and sponsored by the U.S. Department of Energy's Office of Energy Efficiency and Renewable Energy. We acknowledge the National Renewable Energy Laboratory's Optical Biophysics Facility and Laboratory Manager Carolyn E. Lubner for assistance in the set-up and use of the ultrafast TA spectroscopy instrumentation. G.D. thanks Louis. E. Brus for teaching her how to be a scientist.

AUTHOR DECLARATIONS

Conflict of Interest

The authors have no conflicts to disclose.

Author Contributions

Katherine E. Shulenberger: Conceptualization (equal); Formal analysis (lead); Investigation (lead); Methodology (lead); Resources (supporting); Software (lead); Visualization (lead); Writing – original draft (equal); Writing – review & editing (supporting). **Skylar J. Sherman:** Conceptualization (supporting); Investigation (supporting); Writing – review & editing (supporting). **Madison R. Jilek:** Investigation (supporting); Writing – review & editing (supporting). **Helena R. Keller:** Resources (lead); Writing – review & editing (supporting). **Lauren M. Pellows:** Investigation (supporting); Writing – review & editing (supporting). **Gordana Dukovic:** Conceptualization (equal); Funding acquisition (lead); Project administration (lead); Supervision (lead); Writing – original draft (equal); Writing – review & editing (lead).

DATA AVAILABILITY

The data that support the findings of this study are available from the corresponding author upon reasonable request.

REFERENCES

- ¹J. M. Pietryga, Y.-S. Park, J. Lim, A. F. Fidler, W. K. Bae, S. Brovelli, and V. I. Klimov, *Chem. Rev.* **116**, 10513 (2016).
- ²V. I. Klimov, J. A. McGuire, R. D. Schaller, and V. I. Rupasov, *Phys. Rev. B* **77**, 195324 (2008).
- ³V. I. Klimov, A. A. Mikhailovsky, D. W. McBranch, C. A. Leatherdale, and M. G. Bawendi, *Science* **287**, 1011 (2000).
- ⁴B. Fisher, J.-M. Caruge, Y.-T. Chan, J. Halpert, and M. G. Bawendi, *Chem. Phys.* **318**, 71 (2005).
- ⁵A. Pandey and P. Guyot-Sionnest, *J. Chem. Phys.* **127**, 111104 (2007).
- ⁶G. Nair, L.-Y. Chang, S. M. Geyer, and M. G. Bawendi, *Nano Lett.* **11**, 2145 (2011).
- ⁷M. C. Beard, *J. Phys. Chem. Lett.* **2**, 1282 (2011).
- ⁸R. J. Ellingson, M. C. Beard, J. C. Johnson, P. Yu, O. I. Micic, A. J. Nozik, A. Shabaev, and A. L. Efros, *Nano Lett.* **5**, 865 (2005).
- ⁹H. Zhu, N. Song, W. Rodriguez-Cordoba, and T. Lian, *J. Am. Chem. Soc.* **134**, 4250 (2012).
- ¹⁰E. Y. Tsui, K. H. Hartstein, and D. R. Gamelin, *J. Am. Chem. Soc.* **138**, 11105 (2016).
- ¹¹J. D. Rinehart, A. M. Schimpf, A. L. Weaver, A. W. Cohn, and D. R. Gamelin, *J. Am. Chem. Soc.* **135**, 18782 (2013).
- ¹²K. E. Shulenberger, H. R. Keller, L. M. Pellows, N. L. Brown, and G. Dukovic, *J. Phys. Chem. C* **125**, 22650 (2021).
- ¹³Y. Yang, W. Rodríguez-Córdoba, and T. Lian, *Nano Lett.* **12**, 4235 (2012).
- ¹⁴I. Tanghe, J. Llusar, J. I. Climente, A. Barker, G. Paternò, F. Scotognella, A. Polovitsyn, A. H. Khan, Z. Hens, D. Van Thourhout, P. Geiregat, and I. Moreels, *Adv. Opt. Mater.* **10**, 2201378 (2022).
- ¹⁵S. Bisschop, P. Geiregat, T. Aubert, and Z. Hens, *ACS Nano* **12**, 9011 (2018).
- ¹⁶R. R. Cooney, S. L. Sewall, D. M. Sagar, and P. Kambhampati, *Phys. Rev. Lett.* **102**, 127404 (2009).
- ¹⁷N. Ahn, C. Livache, V. Pinchetti, H. Jung, H. Jin, D. Hahn, Y.-S. Park, and V. I. Klimov, *Nature* **617**, 79 (2023).
- ¹⁸V. I. Klimov, S. A. Ivanov, J. Nanda, M. Achermann, I. Bezel, J. A. McGuire, and A. Piryatinski, *Nature* **447**, 441 (2007).
- ¹⁹V. I. Klimov, A. A. Mikhailovsky, S. Xu, A. Malko, J. A. Hollingsworth, C. A. Leatherdale, H. J. Eisler, and M. G. Bawendi, *Science* **290**, 314 (2000).
- ²⁰K. Wu, Y.-S. Park, J. Lim, and V. I. Klimov, *Nat. Nanotechnol.* **12**, 1140 (2017).
- ²¹V. I. Klimov, *Annu. Rev. Phys. Chem.* **58**, 635 (2007).
- ²²C. Melnychuk and P. Guyot-Sionnest, *Chem. Rev.* **121**, 2325 (2021).
- ²³S. L. Sewall, A. Franceschetti, R. R. Cooney, A. Zunger, and P. Kambhampati, *Phys. Rev. B* **80**, 081310 (2009).
- ²⁴V. Klimov, S. Hunsche, and H. Kurz, *Phys. Rev. B* **50**, 8110 (1994).
- ²⁵J. Huang, Z. Huang, Y. Yang, H. Zhu, and T. Lian, *J. Am. Chem. Soc.* **132**, 4858 (2010).
- ²⁶R. D. Schaller, M. Sykora, S. Jeong, and V. I. Klimov, *J. Phys. Chem. B* **110**, 25332 (2006).
- ²⁷R. D. Schaller, M. A. Petruska, and V. I. Klimov, *Appl. Phys. Lett.* **87**, 253102 (2005).
- ²⁸C. Qin, J. Guo, Z. Zhou, Y. Liu, and Y. Jiang, *Nanotechnology* **32**, 185701 (2021).
- ²⁹H. Zhu, Y. Yang, and T. Lian, *Acc. Chem. Res.* **46**, 1270 (2013).
- ³⁰A. L. Efros, M. Rosen, M. Kuno, M. Nirmal, D. J. Norris, and M. Bawendi, *Phys. Rev. B* **54**, 4843 (1996).
- ³¹T. Labrador and G. Dukovic, *J. Phys. Chem. C* **124**, 8439 (2020).
- ³²A. Franceschetti and Y. Zhang, *Phys. Rev. Lett.* **100**, 136805 (2008).
- ³³N. Lenngren, T. Garting, K. Zheng, M. Abdellah, N. Lascoux, F. Ma, A. Yartsev, K. Židek, and T. Pullerits, *J. Phys. Chem. Lett.* **4**, 3330 (2013).
- ³⁴M. N. Ashner, K. E. Shulenberger, F. Krieg, E. R. Powers, M. V. Kovalenko, M. G. Bawendi, and W. A. Tisdale, *ACS Energy Lett.* **4**, 2639 (2019).
- ³⁵Y. Li, Y. Han, W. Liang, B. Zhang, Y. Li, Y. Liu, Y. Yang, K. Wu, and J. Zhu, *Nat. Commun.* **13**, 5559 (2022).
- ³⁶I. Gdor, A. Shapiro, C. Yang, D. Yanover, E. Lifshitz, and S. Ruhman, *ACS Nano* **9**, 2138 (2015).
- ³⁷H. Tahara, M. Sakamoto, T. Teranishi, and Y. Kanemitsu, *Nat. Commun.* **9**, 3179 (2018).
- ³⁸K. J. Karki, F. Ma, K. Zheng, K. Zidek, A. Mousa, M. A. Abdellah, M. E. Messing, L. R. Wallenberg, A. Yartsev, and T. Pullerits, *Sci. Rep.* **3**, 2287 (2013).
- ³⁹B. O. Dabbousi, J. Rodriguez-Viejo, F. V. Mikulec, J. R. Heine, H. Mattoussi, R. Ober, K. F. Jensen, and M. G. Bawendi, *J. Phys. Chem. B* **101**, 9463 (1997).
- ⁴⁰H. H.-Y. Wei, C. M. Evans, B. D. Swartz, A. J. Neukirch, J. Young, O. V. Prezhdo, and T. D. Krauss, *Nano Lett.* **12**, 4465 (2012).
- ⁴¹N. C. Anderson, M. P. Hendricks, J. J. Choi, and J. S. Owen, *J. Am. Chem. Soc.* **135**, 18536 (2013).
- ⁴²Y. Gao and X. Peng, *J. Am. Chem. Soc.* **137**, 4230 (2015).
- ⁴³D. R. Baker and P. V. Kamat, *Langmuir* **26**, 11272 (2010).
- ⁴⁴M. Abdellah, K. J. Karki, N. Lenngren, K. Zheng, T. Pascher, A. Yartsev, and T. Pullerits, *J. Phys. Chem. C* **118**, 21682 (2014).
- ⁴⁵O. M. Pearce, J. S. Duncan, N. H. Damrauer, and G. Dukovic, *J. Phys. Chem. C* **122**, 17559 (2018).
- ⁴⁶I. Mekis, D. V. Talapin, A. Kornowski, M. Haase, and H. Weller, *J. Phys. Chem. B* **107**, 7454 (2003).
- ⁴⁷W. W. Yu, L. H. Qu, W. Z. Guo, and X. G. Peng, *Chem. Mater.* **15**, 2854 (2003).
- ⁴⁸L. Amirav and A. P. Alivisatos, *J. Phys. Chem. Lett.* **1**, 1051 (2010).
- ⁴⁹H. W. Tseng, M. B. Wilker, N. H. Damrauer, and G. Dukovic, *J. Am. Chem. Soc.* **135**, 3383 (2013).
- ⁵⁰U. Megerle, I. Pugliesi, C. Schrieffer, C. F. Sailer, and E. Riedle, *Appl. Phys. B* **96**, 215 (2009).
- ⁵¹S. A. Kovalenko, A. L. Dobryakov, J. Ruthmann, and N. P. Ernstring, *Phys. Rev. A* **59**, 2369 (1999).
- ⁵²S. A. Kovalenko, N. P. Ernstring, and J. Ruthmann, *Chem. Phys. Lett.* **258**, 445 (1996).
- ⁵³M. N. Ashner, S. W. Winslow, J. W. Swan, and W. A. Tisdale, *J. Phys. Chem. A* **123**, 3893 (2019).
- ⁵⁴K. E. Shulenberger, T. S. Bischof, J. R. Caram, H. Utzat, I. Coropceanu, L. Nienhaus, and M. G. Bawendi, *Nano Lett.* **18**, 5153 (2018).
- ⁵⁵D. J. Norris and M. G. Bawendi, *Phys. Rev. B* **53**, 16338 (1996).
- ⁵⁶A. L. Efros and M. Rosen, *Annu. Rev. Mater. Sci.* **30**, 475 (2000).
- ⁵⁷A. I. Ekimov, I. A. Kudryavtsev, A. L. Efros, T. V. Yazeva, F. Hache, M. C. Schanne-Klein, A. V. Rodina, D. Ricard, and C. Flytzanis, *J. Opt. Soc. Am. B* **10**, 100 (1993).
- ⁵⁸I. Robel, R. Gresback, U. Kortshagen, R. D. Schaller, and V. I. Klimov, *Phys. Rev. Lett.* **102**, 177404 (2009).
- ⁵⁹Y. Z. Hu, S. W. Koch, M. Lindberg, N. Peyghambarian, E. L. Pollock, and F. F. Abraham, *Phys. Rev. Lett.* **64**, 1805 (1990).
- ⁶⁰F. Sousa Velosa, H. Van Avermaet, P. Schiettecatte, L. Mingabudinova, P. Geiregat, and Z. Hens, *Adv. Opt. Mater.* **10**, 2200328 (2022).
- ⁶¹C. Zhang, T. N. Do, X. Ong, Y. Chan, and H.-S. Tan, *Chem. Phys.* **481**, 157 (2016).
- ⁶²S. L. Sewall, R. R. Cooney, K. E. H. Anderson, E. A. Dias, D. M. Sagar, and P. Kambhampati, *J. Chem. Phys.* **129**, 084701 (2008).
- ⁶³S. L. Sewall, R. R. Cooney, E. A. Dias, P. Tyagi, and P. Kambhampati, *Phys. Rev. B* **84**, 235304 (2011).
- ⁶⁴C. Y. Wong and G. D. Scholes, *J. Phys. Chem. A* **115**, 3797 (2011).
- ⁶⁵G. Lubin, G. Yaniv, M. Kazes, A. C. Ulku, I. M. Antolovic, S. Burri, C. Bruschini, E. Charbon, V. J. Yallapragada, and D. Oron, *ACS Nano* **15**, 19581 (2021).
- ⁶⁶Y. Xie, N. Du, S. Yu, L. Zhang, and M. Yang, *J. Phys. Chem. C* **123**, 30714 (2019).
- ⁶⁷D. F. Underwood, T. Kippeny, and S. J. Rosenthal, *J. Phys. Chem. B* **105**, 436 (2001).
- ⁶⁸M. D. Garrett, M. J. Bowers, J. R. McBride, R. L. Orndorff, S. J. Pennycook, and S. J. Rosenthal, *J. Phys. Chem. C* **112**, 436 (2008).
- ⁶⁹V. I. Klimov, C. J. Schwarz, D. W. McBranch, C. A. Leatherdale, and M. G. Bawendi, *Phys. Rev. B* **60**, R2177 (1999).
- ⁷⁰K. J. Schnitzenbaumer, T. Labrador, and G. Dukovic, *J. Phys. Chem. C* **119**, 13314 (2015).
- ⁷¹E. A. McArthur, A. J. Morris-Cohen, K. E. Knowles, and E. A. Weiss, *J. Phys. Chem. B* **114**, 14514 (2010).

- ⁷²J. D. Keene, J. R. McBride, N. J. Orfield, and S. J. Rosenthal, *ACS Nano* **8**, 10665 (2014).
- ⁷³K. E. Knowles, E. A. McArthur, and E. A. Weiss, *ACS Nano* **5**, 2026 (2011).
- ⁷⁴B. Shakeri and R. W. Meulenber, *Langmuir* **31**, 13433 (2015).
- ⁷⁵A. Lesiak, M. Banski, K. Halicka, J. Cabaj, A. Żak, and A. Podhorodecki, *Nanotechnology* **32**, 075705 (2021).
- ⁷⁶S. Jeong, M. Achermann, J. Nanda, S. Ivanov, V. I. Klimov, and J. A. Hollingsworth, *J. Am. Chem. Soc.* **127**, 10126 (2005).
- ⁷⁷S. F. Wuister, C. de Mello Donegá, and A. Meijerink, *J. Phys. Chem. B* **108**, 17393 (2004).
- ⁷⁸S. He, Q. Li, T. Jin, and T. Lian, *J. Chem. Phys.* **156**, 054704 (2022).
- ⁷⁹G. Grimaldi, J. J. Geuchies, W. van der Stam, I. du Fossé, B. Brynjarsson, N. Kirkwood, S. Kinge, L. D. A. Siebbeles, and A. J. Houtepen, *Nano Lett.* **19**, 3002 (2019).
- ⁸⁰D. V. Talapin, A. L. Rogach, A. Kornowski, M. Haase, and H. Weller, *Nano Lett.* **1**, 207 (2001).
- ⁸¹G. W. Bryant and W. Jaskolski, *J. Phys. Chem. B* **109**, 19650 (2005).
- ⁸²S. J. W. Vonk, B. A. J. Heemskerk, R. C. Keitel, S. O. M. Hinterding, J. J. Geuchies, A. J. Houtepen, and F. T. Rabouw, *Nano Lett.* **21**, 5760 (2021).
- ⁸³V. Türck, S. Rodt, O. Stier, R. Heitz, R. Engelhardt, U. W. Pohl, D. Bimberg, and R. Steingrüber, *Phys. Rev. B* **61**, 9944 (2000).
- ⁸⁴H. P. Wagner, H. P. Tranitz, H. Preis, W. Langbein, K. Leosson, and J. M. Hvam, *Phys. Rev. B* **60**, 10640 (1999).
- ⁸⁵G. Lubin, R. Tenne, A. C. Ulku, I. M. Antolovic, S. Burri, S. Karg, V. J. Yallapragada, C. Bruschini, E. Charbon, and D. Oron, *Nano Lett.* **21**, 6756 (2021).
- ⁸⁶H. Seiler, S. Palato, C. Sonnichsen, H. Baker, and P. Kambhampati, *Nano Lett.* **18**, 2999 (2018).
- ⁸⁷B. Patton, W. Langbein, and U. Woggon, *Phys. Rev. B* **68**, 125316 (2003).
- ⁸⁸C. Y. Wong and G. D. Scholes, *J. Lumin.* **131**, 366 (2011).
- ⁸⁹M. C. Tropicovsky and A. Franceschetti, *Appl. Phys. Lett.* **87**, 263115 (2005).
- ⁹⁰A. Franceschetti and Tropicovsky, *J. Phys. Chem. C* **111**, 6154 (2007).
- ⁹¹T. Takagahara, *Phys. Rev. B* **39**, 10206 (1989).